RSC Publishing PCCP

Tin oxide-surface modified anatase titanium(IV) dioxide with enhanced UV-light photocatalytic activity

Journal:	*Physical Chemistry Chemical Physics*
Manuscript ID:	CP-ART-08-2011-022708
Article Type:	Paper
Date Submitted by the Author:	24-Aug-2011
Complete List of Authors:	Tada, Hiroaki; Kinki University, Molecular Engineering Institute Fujishima, Musashi; Kinki University, Department of Applied Chemistry Nolan, Michael; University College Cork, Department of Chemistry Yamamoto, Hironori; Kinki University, Department of Applied Chemistry Jin, Qiliang; Kinki University, Department of Applied Chemistry

PCCP's high standards

August 2011: *Physical Chemistry Chemical Physics* (*PCCP*) is a high quality journal with a large international readership from many communities

Only very important, insightful and high-quality work should be recommended for publication in *PCCP*.

To merit acceptance in *PCCP* - a manuscript must report:

- Very high quality, reproducible new work
- **Important new physical insights** of significant general interest
- A novel, stand-alone contribution

Routine or incremental work should not be recommended for publication. Purely synthetic work is not suitable for *PCCP.*

If you rate the article as 'routine' yet recommend acceptance, please give specific reasons in your report.

Less than 50% of articles sent for peer review are recommended for publication in *PCCP*. The current *PCCP* Impact Factor 3.45.

PCCP is proud to be a leading journal. We thank you very much for your help in evaluating this manuscript. Your advice as a referee is greatly appreciated.

With our best wishes,

Philip Earis (pccp@rsc.org)
Editor, *Physical Chemistry Chemical Physics*

Pekka Pyykko
Chair, Editorial Board

General Guidance (For further details, see the RSC's Refereeing Procedure and Policy)

Referees have the responsibility to treat the manuscript as confidential. Please be aware of our **Ethical Guidelines** which contain full information on the responsibilities of referees and authors.

When preparing your report, please:

- Comment on the originality, importance, impact and scientific reliability of the work;
- State clearly whether you would like to see the paper accepted or rejected and give detailed comments (with references, as appropriate) that will both help the Editor to make a decision on the paper and the authors to improve it;

Please inform the Editor if:

- There is a conflict of interest;
- There is a significant part of the work which you cannot referee with confidence;
- If the work, or a significant part of the work, has previously been published, including online publication, or if the work represents part of an unduly fragmented investigation.

When submitting your report, please:

- Provide your report rapidly and within the specified deadline, or inform the Editor immediately if you cannot do so. We welcome suggestions of alternative referees.

Tin oxide-surface modified anatase titanium(IV) dioxide with enhanced UV-light photocatalytic activity

Musashi Fujishima,[a] Qiliang Jin,[a] Hironori Yamamoto,[a] Hiroaki Tada[a]* and Michael Nolan[b]*

Received (in XXX, XXX) Xth XXXXXXXXX 200X, Accepted Xth XXXXXXXXX 200X
First published on the web Xth XXXXXXXXX 200X
DOI: 10.1039/b000000x

$[Sn(acac)_2]Cl_2$ is chemisorbed on the surfaces of anatase TiO_2 via ion-exchange between the complex ions and H^+ released from the surface Ti-OH groups without liberation of the acetylacetonate ligand ($Sn(acac)_2/TiO_2$). The post-heating at 873 K in air forms tin oxide species on the TiO_2 surface in a highly dispersion state at a molecular scale ($(SnO_2)_m/TiO_2$). A low level of this *p* block metal oxide surface modification (~ 0.007 Sn ions nm^{-2}) accelerates the UV-light-activities for the liquid- and gas-phase reactions, whereas in contrast to the surface modification with *d* block metal oxides such as FeO_x and NiO, no visible-light response is induced. Electrochemical measurements and first principles density functional theory (DFT) calculations for $(SnO_2)_m/TiO_2$ model clusters (m = 1, 2) indicate that the bulk (TiO_2)-to-surface interfacial electron transfer (BS-IET) enhances charge separation and the following electron transfer to O_2 to increase the photocatalytic activity.

1. Introduction

Recent intensive researches for developing semiconductor photocatalysts have opened up avenues for environmental purification and solar energy conversion into electric or chemical energy.[1,2] Among many kinds of semiconductor photocatalysts, TiO_2 is one of the most promising because of its high oxidation power, high photostability, relative abundance in nature and nontoxicity.[3,4] The key to improve its photocatalytic activity lies on increasing the efficiency of charge separation through the suppression of charge recombination. One of the strategies for this is to form the heterojunction between TiO_2 and partner semiconductors[5-8] or metals.[9] Previously, we reported that a patterned bilayer-type heterojunction system composing of the TiO_2 overlayer and the fluorine-doped SnO_2 ($F:SnO_2$) underlayer has a high photocatalytic activity for the decomposition of acetaldehyde under UV-light irradiation.[10] This effect results from the efficient bulk-to-bulk interfacial electron transfer from the TiO_2 overlayer to the underlying $F:SnO_2$ film. The photocatalytic activity of the heterojunction system depends on the relative positions of the conduction band (CB) and valence band (VB) edges of TiO_2 and $F:SnO_2$. In order to construct the heterojunction system with suitable energy band alignments, the surface modification technique named chemisorption-calcination (CC), is very effective.[11] In this technique, chemisorption of metal complexes on the TiO_2 surface with successive calcination yields metal oxide species highly dispersed on the surface at a molecular scale. Recently, we have shown that the surface modification of TiO_2 with iron oxide-[12,13] and nickel oxide[14] using this technique gives rise to a high level of activities under illumination of both visible- and UV-light.

Here we report the UV-light-activity of tin oxide-surface modified TiO_2 ($(SnO_2)_m/TiO_2$) prepared by the CC technique. The formation mechanism of $(SnO_2)_m/TiO_2$ and the surface modification effect on the photocatalytic activity for liquid- and gas-phase test reactions are discussed. First principles density functional theory (DFT) simulations of small SnO_2 species adsorbed at the anatase (001) surfaces are presented to provide insights into the experimental findings.

2. Experimental

2.1 Sample preparation

Anatase TiO_2 particles (ST-01 with specific surface area = 309 $m^2\ g^{-1}$, A-100 with specific surface area = 8.1 $m^2\ g^{-1}$, Ishihara Sangyo) were used as a standard photocatalyst. By the CC technique utilizing this reaction, $(SnO_2)_m/TiO_2$ was prepared as follows: After TiO_2 particles (1 g) had been added to 50 mL of a $[Sn(acac)_2]Cl_2$ ethanol solution, they were allowed to stand for 24 h at 298 K. The $[Sn(acac)_2]Cl_2$ concentration was changed from 1.6×10^{-7} mol dm^{-3} to 1.0 ×

10^{-4} mol dm^{-3}. The solid samples were separated by centrifugation and washed twice with the solvent for the physisorbed complexes to be removed. Then, they were dried in vacuum at room temperature, followed by heating in air at 873 K for 1 h. For electrochemical measurements, mesoporous TiO_2 nanocrystalline film electrodes were used. A paste containing anatase TiO_2 particles with a mean size of 20 nm (PST-18NR, Nikki Syokubai Kasei) was coated on F:SnO_2-film coated glass substrates (12 Ω/□) by a squeegee method, and the sample was heated in air at 773 K to form mesoporous-TiO_2 films (mp-TiO_2/FTO).

2.2 Adsorption measurements

The adsorption process of $[Sn(acac)_2]Cl_2$ on TiO_2 particles (ST-01) was examined by following the change of the electronic absorption spectra with different amount of the TiO_2 particles dispersed in 1×10^{-4} mol dm^{-3} $[Sn(acac)_2]Cl_2$ ethanol solution (50 mL) at 298 K for 24 h. Adsorption isotherms of Sn^{4+} ions were obtained by exposing TiO_2 particles (2 g) to ethanol solutions with different concentrations of $Sn(acac_2)Cl_2$ (50 mL). After the particles were separated from the suspension in both the experiments by centrifugation, the concentrations of $[Sn(acac)_2]Cl_2$ was determined from the absorbance at 274.5 nm (ε_{max} = 1.54 × 10^4 mol^{-1} dm cm^{-1}) with a Hitachi U-4000 spectrophotometer. The pH measurement was also performed on the supernatant (5 mL) diluted with 10 mL water after the former experiment.

2.3 Sample characterization

The Sn loading amount was determined by inductively coupled plasma spectroscopy (ICPS-7510, Shimadzu). The sample (0.1 g) was dispersed to hot conc. H_2SO_4 (20 mL), and the deposits were thoroughly dissolved into the solution by stirring. The solution was diluted 5 times in volume with water, and then the Sn concentration was measured. UV-vis diffuse reflectance spectrum of $(SnO_2)_m/TiO_2$ (A-100) was recorded on a Hitachi U-4000 spectrophotometer. The spectrum was converted to the absorption spectrum by using the Kubelka-Munk function. Diffuse reflectance Fourier transform infrared (DRIFT) spectra of the particles (ST-01) diluted 25 wt % with KBr (spectroscopic grade, > 98 %, Kanto Chemical) were obtained with a JASCO FT/IR-470plus spectrometer equipped with a diffuse reflectance attachment (Spectra Tech, Inc.). In order to determine number of acetylacetonate ligands in the complex-adsorbed ST-01, thermogravimetric analysis (TG)/differential thermal analysis (DTA) was conducted with a thermal analyzer (TG8010D, Rigaku) using dried samples in air by increasing temperature from 293 to 1,273 K at a heating rate of 10 K min^{-1}. Transmission electron microscopic (TEM) observation and energy dispersive X-ray (ED) spectroscopic measurements were performed using a JEOL JEM-3000F and Gatan Imaging Filter at an applied voltage of 300kV. X-ray photoelectron spectroscopic (XPS) measurements were performed using a Kratos Axis Nova X-ray photoelectron spectrometer with a monochromated Al K_α X-ray source ($h\nu$ = 1486.6 eV) operated at 15 kV and 10 mA. The take-off angle was 90º, and multiplex spectra were obtained for Sn_{3d}, O_{1s}, and Ti_{2p} photopeaks. All the binding energies (E_B) were referenced with respect to the C_{1s} at 284.6 eV. The electrochemical properties of the $(SnO_2)_m$-surface modified mp-TiO_2/FTO electrodes ($(SnO_2)_m$/mp-TiO_2/FTO) were measured in 0.1 mol dm^{-3} $NaClO_4$ aqueous solution in a regular three-electrode electrochemical cell using a galvanostat/potentiostat (HZ-5000, Hokuto Denko). Glassy carbon and an Ag/AgCl electrode (TOA-DKK) were used as a counter electrode and a reference electrode, respectively.

2.4 Photocatalytic activity evaluation

In both the decomposition of acetaldehyde (CH_3CHO) and 2-naphthol (2-NAP), the reaction cells were irradiated with a Xe lamp (Wacom HX-500) through two pieces of FTO-coated glass transmitting the light of $330 < \lambda < 400$ nm for the UV-light photocatalytic activity evaluation and through a cut off filter (L-42 (Toshiba) transmitting the light of $\lambda > 400$ nm for the visible-light activity evaluation. A 596 ppm standard CH_3CHO gas (CH_3CHO/N_2) was introduced into the reaction chamber to be diluted with air such that its initial concentration was kept within the 400 ppm range. After the adsorption equilibrium of CH_3CHO on A-100 or $(SnO_2)_m$/A-100 particles (0.05 g) had been achieved under dark conditions, irradiation was carried out at room temperature. The concentration of CH_3CHO was determined as a function of time by gas chromatography (GC-2014, Shimadzu) with a SHINCARBON A f.i.d. column (1.6 mmϕ × 3.1 m): injection and column temperatures were 363 K and 343 K, respectively, and N_2 was used as a carrier gas. A-100 or $(SnO_2)_m$/A-100 particles (0.01 g) was placed in 50 mL of 4.0×10^{-5} mol dm^{-3} solution of 2-NAP (solvent, acetonitrile : water = 1 : 99 v/v) in a borosilicate glass container was irradiated. 2 mL of the solution was sampled every 10 min and the electronic absorption spectra of the reaction solutions were measured using a spectrometer (UV-1800, Shimadzu) to determine 2-NAP concentration from the absorption peak at 224 nm.

2.5 SnO_2-TiO_2 Calculations

To model the anatase (001) surfaces, we use a three dimensional periodic slab model and a plane wave basis set to describe the valence electronic wave functions within the VASP code.[15] The cut-off for the kinetic energy is 396 eV. For the core-valence interaction we apply Blöchl's projector augmented wave (PAW) method,[16] with Ti described by 4 valence electrons and oxygen by 6 valence electrons; Sn is described with 4 valence electrons. We use the Perdew-Wang91 approximation to the exchange-correlation functional.[17] *k*-point sampling is performed using the Monkhorst-Pack scheme, with a (2 × 2 × 1) sampling grid for both surfaces.

For describing the electronic states of Ti in TiO_2, we have used the DFT+U approach. DFT+U[18,19] adds a Hubbard U correction to describe reduced metal cation states, such as Ti^{3+}. From the literature, values of U in the range 3 – 5 eV are

reasonable[20-23] and we apply U = 4.5 eV to the Ti 3d states throughout this paper.[24,25] For Sn, no +U correction is applied, since the electronic states are reasonably well described with DFT. While DFT+U fixes some of the problems with DFT in describing partially filled *d* states, it still does not repair the band gap underestimation inherent in approximate DFT and the energy gaps resulting from this work will be underestimated compared with experiment and will show some dependence on the precise DFT+U setup; our DFT+U set up uses robust parameters from the author's own work and from the literature[20-25] and we are primarily interested in qualitative changes in the energy gap as a result of modification of the TiO_2 surface with the metal oxide nanoclusters.

The bulk lattice constants of anatase TiO_2 have been computed by fitting a set of constant volume DFT+U energies to a Murnaghan equation of state, giving the following bulk lattice constants: $a = b = 4.172$ Å, $c = 9.627$ Å. The anatase (101) surface is the most stable, as measured by surface energy;[26] however, the (001) surface can be produced in expermients and has been well studied.[27,28] The (001) surface is oxygen terminated and shows 5-fold coordinated Ti at the surface. The terminating oxygen are two coordinate, with the next oxygen subsurface layer showing 3 coordinated oxygen. For (001), a (1 × 4) reconstruction is stable,[29] but in this work it is sufficient to consider an unreconstructed surface model. A (4 × 2) surface supercell is employed for for anatase (001); these surface supercell expansions are large enough to allow for adsorption of essentially isolated clusters. The anatase surface slab is 8 O-Ti-O layers thick, with all surfaces having a vacuum gap of 12 Å. The bottom trilayer in each surface is held fixed and all other layers are allowed relax. The convergence in the wavefunction relaxation is 0.0001 eV, while the ionic relaxation is converged when the forces on the atoms are less than 0.02 eV/ Å. Fermi level smearing with the Methfessel Paxton scheme is applied, with $\sigma = 0.1$ eV. All calculations are spin polarised.

The bare TiO_2 surface, the metal oxide clusters adsorbed at TiO_2 and the free metal oxide clusters are calculated in the same periodic supercell, with the same plane wave cut off energy, the same *k*-point sampling grid and the same PAW potentials, ensuring consistency between calculations. To study cluster adsorption, the SnO_x clusters are positioned in a number of configurations at the surface and a full relaxation is performed within a fixed supercell. Some short ab initio molecular dynamics simulations in the NVE ensemble with a 0.1 fs timestep at 600 K have been run for 2 ps, with no change in the adsorption structure. The adsorption energy is computed from

$$E^{ads} = E((SnO_x)\text{-}TiO_2) - \{ E(SnO_x) + E(TiO_2) \} \quad (1)$$

Where $E((SnO_x)_m\text{-}TiO_2)$ is the total energy of the SnO_x cluster supported on the TiO_2 surface, and $E(SnO_x)$ and $E(TiO_2)$ are the total energies of the free SnO_x cluster (where SnO_x indicates that Sn can be in a +4 or +2 oxidation state) and the bare surface; a negative adsorption energy signifies that cluster adsorption is stable.

In the DOS plots, a smearing of 0.1 eV is used and the cluster DOS are scaled by a factor of 10 to allow for the fact that the cluster contains a maximum 4 cations and 8 anions, compared to a maximum of 96 surface cations and 192 surface anions in rutile (110) to prevent the surface DOS swamping the cluster DOS if the scaling was not applied.

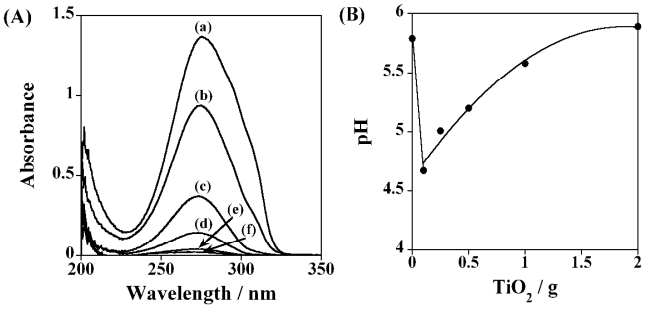

Fig. 1 (A) UV-Vis absorption spectra of a 1×10^{-4} mol dm^{-3} $Sn(acac)_2Cl_2$ solution without ST-01 (a), with addition of ST-01 (b) 0.1 g, (c) 0.25 g, (d) 0.5 g, (e) 1 g, (f) 2 g. (B) Plots of the solution pH vs. amount of ST-01 added.

3. Results and discussion

3.1 Experimental results

$[Sn(acac)_2]Cl_2$ has an absorption assigned to the π-π^* transition in the acetylacetonate (acac)-ligand at 275 nm.[30] Fig. 1A shows UV-vis absorption spectra of a 1×10^{-4} mol dm^{-3} $[Sn(acac)_2]Cl_2$ solution and the solutions equilibrated with various amounts of ST-01. As the amount of ST-01 increases, the absorption intensity monotonically weakens, while no absorption of acetylacetone (AcacH) at 272 nm appears during the adsorption. Fig. 1B presents the relationship between the amount of ST-01 added and pH of the supernatant. On adding 0.1 g ST-01 to a 1×10^{-4} mol dm^{-3} $[Sn(acac)_2]Cl_2$ solution, a steep drop of pH from 5.79 to 4.67 is observed, followed by a gradual increase up to 5.89 with increasing amount of ST-01.

To study the adsorption state of $[Sn(acac)_2]^{2+}$ on ST-01, diffuse reflectance Fourier transform infrared (DRIFT) spectra

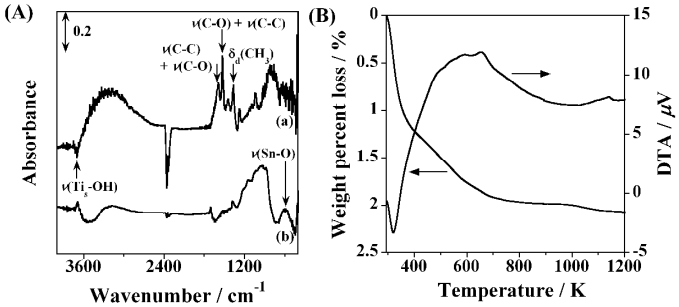

Fig. 2 (A) Difference DRIFT spectra: (a) the complex-adsorbed ST-01 - ST-01; (b) the complex-adsorbed ST-01 after heating at 873 K - ST-01. (B) Thermogravimetric analysis (TG)/differential thermal analysis (DTA) curves of the complex-adsorbed ST-01.

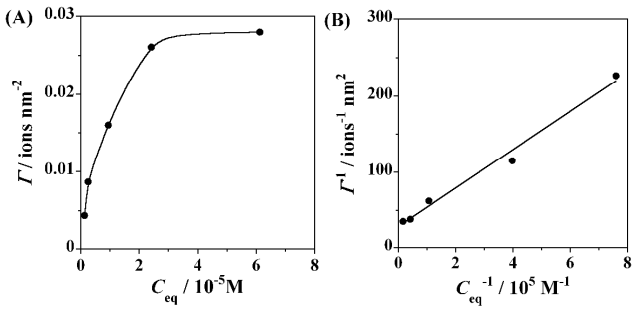

Fig. 3 (A) The adsorption isotherm and (B) the Langmuir plot of $[Sn(acac)_2]Cl_2$ on ST-01 at 298 K.

were measured. Fig. 2A-(a) shows the difference DRIFT spectrum for the complex-adsorbed ST-01 minus ST-01. Three sharp positive peaks are observed at 1589, 1532, and 1364 cm^{-1}, which are assignable to the combination of ν(C-C) + ν(C-O), the combination of ν(C-O) + ν(C-C), and $\delta_s(CH_3)$, respectively.[31] Also, a negative peak due to the surface OH group (Ti_s-OH) appears around 3700 cm^{-1}.[32,33] Fig. 2A-(b) shows the difference DRIFT spectrum for the complex-adsorbed ST-01 after heating at 873 K minus ST-01. All the signals of the acac-ligands disappear, while new positive signals appear at 600 and ca. 3700 cm^{-1} due to the ν(Sn-O) and ν(SnO-H) modes, respectively.[34,35] To estimate the number of the acac-ligands in one complex molecule adsorbed on ST-01, the thermogravimetric analysis (TG)/differential thermal analysis (DTA) was carried out. Fig. 2B shows TG/DTA curves for the complex-adsorbed ST-01 sample. In the TG curve, a rapid decrease in the sample weight up to ca. 373 K is followed by a gradual weight loss to ca. 873 K. The weight loss with an endothermic DTA signal at $T < 373$ K is derived from desorption of the adsorbed water, while that with an exothermic DTA signal at $373 < T < 873$ K is mainly caused by the acac-ligand oxidation. From the latter value, the number of the acac-ligands in the adsorbed complex was calculated to be ca. 2. Also, weight loss with an exothermic DTA signal due to the phase transition from anatase to rutile is observed above 973 K. Consequently, the heating conditions for obtaining tin oxide-surface modified TiO_2 were

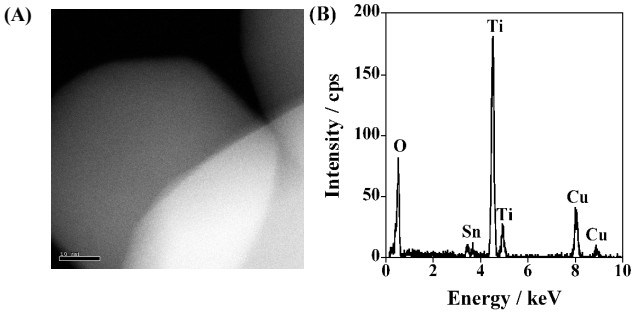

Fig. 4 (A) TEM image (scale bar is 10 nm) and (B) ED spectrum of tin oxide-modified TiO_2.

set at 873 K in air for 1 h.

Further information about the adsorption mechanism can be gained from the adsorption isotherm. Fig. 3A shows the adsorption isotherm of $[Sn(acac)_2]Cl_2$ on ST-01 at 298 K. The loading amount of Sn is expressed by the number of Sn ions per unit TiO_2 surface area (Γ/ions nm^{-2}). The adsorption amount steeply increases with increasing equilibrium concentration (C_{eq}) to be saturated at $C_{eq} > \sim 1 \times 10^5$ mol^{-1} dm^3. The Langmuir plot provides a straight line (Fig. 3B), of

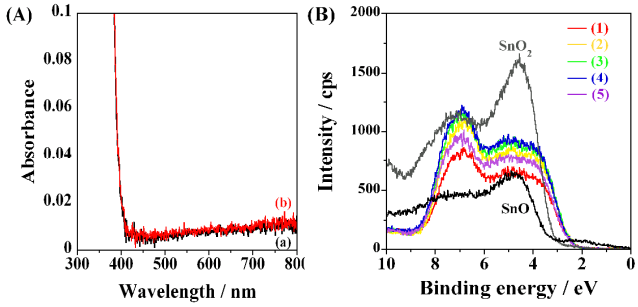

Fig. 5 (A) UV-Vis absorption spectra of (a) A-100 and (b) tin oxide-surface modified A-100 (Γ = 0.024). (B) Valence band-XPS spectra of tin oxide-surface modified A-100 with varying Γ: (1) 0, (2) 0.037, (3) 0.024, (4) 0.0074 and (5) 0.0061, SnO_2 (gray) and SnO (black).

which slope and intercept yield the saturated adsorption amount and equilibrium constant of 0.034 ions nm^{-2} and 1.2×10^5 mol^{-1} dm^3, respectively. Fig. 4 shows the transmission electron microscopic image (A) and energy dispersive X-ray (ED) spectrum (B) of a sample after heating at 873 K (Γ = 0.024 ions nm^{-2}). There exists no observable particle on the TiO_2 surface, while the Sn signals are located at 3.4 and 3.7 keV besides the Ti and O signals in the ED spectrum. The Cu signals arise from the copper grid used for analysis. Evidently, tin oxide species are highly dispersed on anatase TiO_2 as extremely small clusters.

Optical property for the tin oxide-surface modified TiO_2 is of primary importance in connection with its photocatalytic activity. Fig. 5A shows UV-vis absorption spectra of (a) A-100 and (b) tin oxide-surface modified A-100 (Γ = 0.024). Both the samples have strong absorption at $\lambda < 385$ nm due to the interband electronic transition of TiO_2, while almost transparent in the visible range. Similar spectra were obtained also for the other samples with varying Γ. In this manner, modifying TiO_2 with tin oxide species does not promote visible-light absorption, in contrast to FeO_x-[12,13] and NiO[14]-modified TiO_2. In the subsequent section, we present results from the DFT simulations to understand this difference. Further, in order to characterize the tin oxide species on the TiO_2 surface, X-ray photoelectron spectroscopic (XPS) measurements were performed. Fig. 5B shows valence band (VB)-XPS spectra for A-100 with and without the tin oxide-surface modification, and authentic SnO_2 and SnO for comparison. In the VB-XPS spectra of TiO_2, the emission from the O2*p*–VB extends from 2 to 9 eV, while the VBs of SnO_2 and SnO are located in the range from 3 to ~9 eV. Irrespective of Γ, no change in the VB position with the tin oxide modification is appreciated, whereas the VB-tops rise with the surface modification by FeO_x[12] and NiO.[14] Also, in the VB-XPS spectrum of SnO, there exists a Sn 5s band

around 2 eV. However, in the spectra of the tin oxide-surface modified A-100, the Sn5s band is absent in the same manner as the spectrum of SnO_2. This finding suggests that the oxidation state of Sn in the tin oxide species is 4+, and thus the clusters are denoted as $(SnO_2)_m$ below.

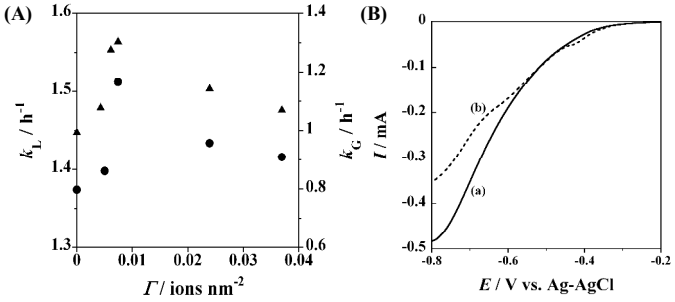

Fig. 6 (A) Plots of the first-order pseudo-constants of the liquid-phase photocatalytic decomposition of 2-NAP (k_L, solid circle) and the gas-phase photocatalitic decomposition of CH_3CHO (k_G, solid triangle) under the illumination of UV-light as a function of Γ. (B) Current-potential curves of (a) $(SnO_2)_m$/mp-TiO_2/FTO and (b) mp-TiO_2/FTO electrodes in an aerated 0.1 mol dm^{-3} $NaClO_4$ aqueous solution in the dark.

On the basis of these results, we propose the mechanism on the formation of the SnO_2 clusters on the TiO_2 surface. Firstly, the adsorption of $[Sn(acac)_2]^{2+}$ ions on the TiO_2 surface occurs through the ion-exchange between the complex ions and H^+ released from the Ti_s-OH groups (eqn 1).

$$[Sn(acac)_2]Cl_2 + 2(Ti_s\text{-}OH) \rightarrow Sn(acac)_2(O\text{-}Ti_s)_2 + 2HCl \quad (1)$$

This process does not involve elimination of the acac-ligands, whereas the adsorptions of $Mg(acac)_2$[11] and $Fe(acac)_3$[13] on TiO_2, and $[VO(acac)_2]$[36] and $[Cr(acac)_3]$[37] on SiO_2 are accompanied by the acac-ligand exchange. Successively, part of the H^+ released is adsorbed on the Ti_s-OH groups forming the Ti_s-OH_2^+ group. The electrostatic repulsion between $[Sn(acac)_2]^{2+}$ ion and the Ti_s-OH_2^+ group prevents further adsorption to reach adsorption equilibrium. From the ZINDO molecular orbital calculations, the molecular cross-sectional area of the complex ion was estimated to be ca. 0.6 nm^2 molecule^{-1}. On the other hand, the area occupied by one complex ion on the TiO_2 surface was estimated from the Langmuir plot to be 29.4 nm^2 ion^{-1}, which is approximately 50 times larger than the molecular cross-sectional area. Secondly, the post-heating process oxidizes the acac-ligands of the adsorbed complex to yield SnO_2 species highly dispersed on the TiO_2 surface (eqn 2).

$$m\text{Sn(acac)}_2(\text{O-Ti}_s)_2 + 25m/2\text{O}_2 \rightarrow (SnO_2)_m/TiO_2 + 7m\text{H}_2\text{O} + 10m\text{CO}_2 \quad (2)$$

Probably, this stems from the strong chemical bond between the complex and the surface to inhibit the aggregation of the SnO_2 species.

To evaluate the photocatalytic activity of $(SnO_2)_m/TiO_2$, the photocatalytic decomposition of 2-NAP and CH_3CHO was examined under illumination of visible-light ($\lambda > 400$ nm, $I_{420\text{-}485\ nm}$ = 1.0 mW cm^{-2}) and UV-light ($330 < \lambda < 400$ nm, $I_{320\text{-}400\ nm}$ = 1.5 mW cm^{-2} for 2-NAP, $I_{320\text{-}400\ nm}$ = 1.0 mW cm^{-2} for CH_3CHO).[38-40] 2-NAP is the starting material of azo-dyes, while CH_3CHO is a volatile organic compound responsible for sick-house syndrome. These compounds were used as model pollutants in water and air. As predicted from the optical property (Fig. 5A), no decompositions occurred under the visible-light irradiation. On the other hand, UV-light irradiation led to the 2-NAP and CH_3CHO decompositions apparently with the first-order kinetics followed. Fig. 6A shows the first-order pseudo-rate constants for the decompositions of 2-NAP (k_L) and CH_3CHO (k_G) under UV-light irradiation as a function of Γ. The plots of both the k_L and k_G exhibit volcano-shaped dependency on Γ with a maximum at $\Gamma \approx 0.0074$ ions nm^{-2}. The SnO_2-surface modification hardly affected the adsorptivity for 2-NAP in the dark at $\Gamma < 0.04$. Certainly, the SnO_2-surface modification has an enhancing effect on the UV-light-activity of TiO_2 for both the liquid- and gas-phase reactions, although the effect is smaller than those by FeO_x[12,13] and NiO[14] surface modification.

In order to obtain the information about the origin of the SnO_2-surface modification effect, current (I)-potential (E) curves were measured for the mp-TiO_2/FTO electrodes in an aerated 0.1 M $NaClO_4$ aqueous solution in the dark. Fig. 6B shows the I-E curves of (a) $(SnO_2)_m$/mp-TiO_2/FTO and (b) mp-TiO_2/FTO electrodes. For both the electrodes, the current due to the O_2 reduction is observed at $E < -0.2$ V, whereas the current hardly flew at $-0.8 < E < -0.2$ V without O_2 (data not shown). Importantly, the reduction current at $E < -0.55$ V is enhanced with the SnO_2-surface modification, i.e., the surface SnO_2 species mediate the electron transfer from TiO_2 to O_2.

3.2 Simulation results

To explore the microscopic mechanisms behind the experimental results, we present the results of DFT+U simulations of models of SnO_2-TiO_2, in which small, molecular sized SnO_2 clusters are adsorbed at TiO_2 surfaces. In an earlier paper we showed that Sn of an Sn_2O_4 cluster adsorbed at rutile (110) surface binds with bridging oxygen from the TiO_2 surface, while O from the cluster binds with 5fold coordinated surface Ti.[41] Fig. 7 presents the atomic structures of SnO_2 and Sn_2O_4 species adsorbed at the anatase (001) surface, where we consider only Sn in its +4 oxidation state, as found in the experiments. The bonding mode is quite different form that with the rutile (110) surface, in which there was little displacement of surface oxygen towards the adsorbate[41]. For the SnO_2 cluster (Fig. 7(a)), Sn from the cluster interacts with two-fold surface terminating oxygen and pulls two of these oxygen atoms out of the surface layer, with displacements of 0.41 and 1.15 Å, resulting in formation of new Sn-O bonds between the cluster and the surface. Oxygen from the cluster interacts with the outermost surface Ti and leads to breaking of the original surface Ti-O bond, the oxygen from this bond is displaced to make the new Sn-O bonds. For the Sn_2O_4 cluster (Fig. 7(b)), it is clear that the

displaced surface oxygen and oxygen from the cluster take the same bonding environment; the surface oxygen atoms are each displaced by 1.11 Å. The adsorption energies are computed to be -3.32 eV for SnO_2 and -5.29 eV for Sn_2O_4, indicating a strong bonding interaction between the cluster and the surface. Maximising the number of new metal-oxygen bonds plays a key role in assuring stability of the adsorbate

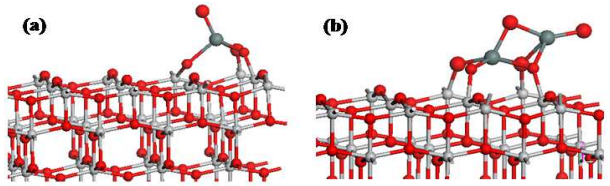

Fig. 7 Atomic structures of SnO_2 species adsorbed at anatase surfaces. (a) SnO_2 anatase (001), (b) Sn_2O_4 anatase (001). In this Fig., surface Ti is the small grey sphere, surface O is the small red ball, Sn from adsorbed SnO_2 is the large dark grey sphere and O from adsorbed SnO_2 is the large red sphere.

structure.

To examine the electronic structure, we plot the projected electronic density of states (PEDOS) for Sn 5s states from the adsorbed SnO_2 species and the Ti 3d states from the anatase (001) surface in Fig. 8. From the PEDOS, we see that, in contrast to other oxides supported on TiO_2,[41] the tin oxide states do not appear inside the TiO_2 energy gap and are in fact found very close to the CB edge of the surface; since the Sn 5s states are unoccupied with an Sn^{4+} oxidation state. For other oxides such as TiO_2,[42] CrO_x and MoO_x,[41] cluster-derived electronic states lie above the VB edge of the surface, pushing the VB edge higher in energy, thus reducing the VB-CB energy gap over the bare surface. In the present system, the SnO_2 and Sn_2O_4-derived states lie well separated from the VB and CB edges of TiO_2 and will not lead to any shift to visible light absorption. These results from the DFT simulations are consistent with the experimental results in Section 3.1, in

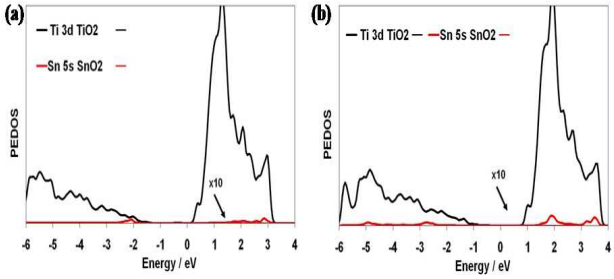

Fig. 8 Electronic DOS projected onto surface Ti 3d states and cluster Sn 5s states for SnO_2 and Sn_2O_4 clusters adsorbed on the anatase (001) surface. (a) anatase (001) SnO_2, (b) anatase (001) Sn_2O_4. The zero of energy is the Fermi level.

which no shift to the visible region was found upon formation of the adsorbed tin oxide species. Another intriguing point is that the Sn5s-derived surface levels are dispersed centred at ~1 eV higher than the CB edge. Upon UV-light excitation, these surface states as well as the CB(TiO_2) can be acceptor levels for the electrons from the VB(TiO_2).

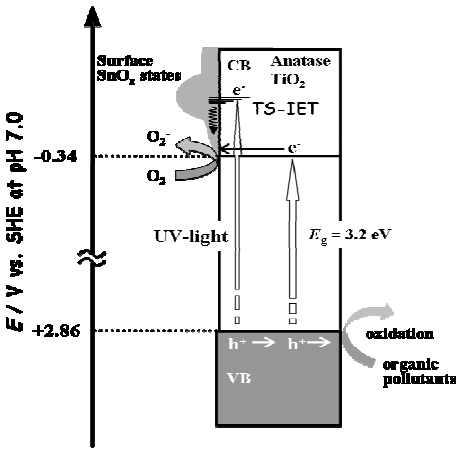

Scheme 1. A Proposed Energy Band Diagram of $(SnO_x)_m/TiO_2$

3.3 Action mechanism of the surface SnO_2 species

On the basis of the experimental and theoretical calculation results, both the enhanced UV activity and lack of visible light activity of anatase TiO_2 with the SnO_2-surface modification (Scheme 1). In the oxidative decomposition of organic compounds, the key to increasing the TiO_2 photocatalytic activity is the efficient transfer of the excited electrons to O_2.[43,44] If SnO_2 species are present at the TiO_2 surface, then upon UV excitation, electrons can be promoted to either the TiO_2 CB or the SnO_2 states around the TiO_2 CB. Excitation of an electron to the SnO_2 states results in separation of electrons and holes, with electrons present on the SnO_2 species. This BS-IET is in contrast to the surface-to-bulk (TiO_2) IET (SB-IET) proposed for the $(FeO_x)_m/TiO_2$[12,13] and NiO/TiO_2[14] systems. A similar IET mechanism has recently been proposed for Cu(II)-grafted TiO_2 to explain its visible-light-activity for 2-propanol decomposition.[45] Further, the surface Sn ions with a low coordination number in small clusters (Fig. 7) can act as an adsorption site for O_2 similarly to the reduced SnO_2 surface facilitating its chemisorption[46] and successive reduction. Consequently, charge recombination is reduced over bare TiO_2, and the holes left in the VB(TiO_2) efficiently oxidize the organic substrates. The excess loading causes the drop of the $E_F(TiO_2)$, decreasing the reducing power of the excited electrons toward O_2.[12] This would explain the presence of the optimum Γ for the photocatalytic activity of $(SnO_2)_m/TiO_2$. Very interestingly, Boppana and Lobo have recently shown that the SnO_x-surface modification of $ZnGa_2O_4$ by an impregnation method significantly increases not only the UV-light-activity but also the visible-light-activity.[47] This finding suggests that the surface modification effect strongly depends on the kind of semiconductors.

4. Conclusions

The CC technique using $[Sn(acac)_2]Cl_2$ as a precursor enables

to form extremely highly dispersed surface tin oxide species on the TiO_2 surface. There is no shift of the absorption edge to the visible region, in contrast to iron oxide- and nickel oxide modified TiO_2, which is explained by the alignments of the TiO_2 and tin oxide electronic states upon formation of the composite material. However, the surface modification increases the UV-light-activities of TiO_2 for both liquid- and gas-phase reactions. This enhancing effect has been shown to originate from the actions of the surface tin oxide species to accept the excited electrons and promote the electron transfer to O_2.

Acknowledgements

The authors express sincere gratitude to Takanori Hattori and Yasutaka Sumida (Nippon Shokubai Co. Ltd.) for helpful discussion. This work was partially supported by a Grant-in-Aid for Scientific Research (B) No. 20350097 from the Ministry of Education, Science, Sport, and Culture, Japan. MN acknowledges support from Science Foundation Ireland (SFI) through the Starting Investigator Research Grant Program, project "EMOIN", grant number SFI 09/SIRG/I1620. We acknowledge computing resources at Tyndall provided by SFI and by the SFI and Higher Education Authority funded Irish Centre for High End Computing

Notes and references

[a] *Department of Applied Chemistry, School of Science and Engineering, Kinki University, 3-4-1, Kowakae, Higashi-Osaka, Osaka 577-8502, Japan*
E-mail: h-tada@apch.kindai.ac.jp

[b] *Tyndall National Institute, Lee Maltings, University College Cork, Cork, Ireland*
E-mail: michael.nolan@tyndall.ie

† Electronic Supplementary Information (ESI) available: [details of any supplementary information available should be included here]. See DOI: 10.1039/b000000x/

1. K. Kalyanasundaram (Ed.), *Dye-Sensitized Solar Cells*, EPFL Press, Lausanne, 2010.
2. C. A. Grimes, O. K. Varghense and S. Ranjan, *Light, Water, Hydrogen The Solar Generation of Hydrogen by Water Photoelectrolysis*, Springer, New York, 2007.
3. A. Fujishima, X. Zhang and D. A. Tryk, *Surf. Sci. Rep.*, 2008, **63**, 515.
4. K. Hashimoto, H. Irie and A. Fujishima, *Jpn. J. Appl. Phys.*, 2005, **44**, 8269.
5. P. V. Kamat, *Chem. Rev.*, 1993, **93**, 267.
6. T. Kawahara, Y. Konishi, H. Tada, N. Tohge, J. Nisii and S. Ito, *Angew. Chem. Int. Ed.*, 2002, **41**, 2811.
7. H. Zhang, G. Chen and D. W. Bahnemann, *J. Mater. Chem.*, 2009, **19**, 5089.
8. G. Liu, L. Wang, H. G. Yang, H.-M. Cheng and G. Q. Lu, *J. Mater. Chem.*, 2010, **20**, 831.
9. H. Tada, T. Kiyonaga and S.-i. Naya, *Chem. Soc. Rev.*, 2009, **38**, 1849.
10. H. Tada, A. Hattori, Y. Tokihisa, K. Imai, N. Tohge and S. Ito, *J. Phys. Chem. B*, 2000, **104**, 4585.
11. H. Tada, M. Yamamoto and S. Ito, *Langmuir* **1999**, *15*, 3699.
12. H. Tada, Q. Jin., H. Nishijima, H. Yamamoto, M. Fujishima, S.-i. Okuoka, T. Hattori, Y. Sumida and H. Kobayashi, *Angew. Chem. Int. Ed.*, 2011, **50**, 3501.
13. Q. Jin, M. Fujishima and H. Tada, *J. Phys. Chem. C*, 2011, **115**, 6478.
14. Q. Jin, T. Ikeda, M. Fujishima and H. Tada, *Chem. Commun.*, 2011, **47**, 8814.
15. (a) G. Kresse and J. Hafner, *Phys. Rev. B,* 1994**, 49**, 14251. (b) G. Kresse and J. Furthmüller, *Comp. Mat. Sci .*, 1996, **6**, 5.
16. (a) P. E. Blöchl, *Phys. Rev. B*, 1994, **50**, 17953. (b) D. Joubert and G. Kresse, *Phys. Rev. B,* 1999, **59**, 1758.
17. J. P. Perdew, J. A. Chevary, S. H. Vosko, K. A. Jackson, M. R. Pederson, D. J. Singh and C. Fiolhais, *Phys. Rev. B.*, 1992, **46**, 6671.
18. V. I. Anisimov, J. Zaanen and O. K. Andersen, *Phys. Rev B*, 1991, **44**, 943.
19. S. L. Dudarev, G. A. Botton, S. Y. Savrasov, C. J. Humphreys and A. P. Sutton, *Phys. Rev. B*, 1998, **57**, 1505.
20. B. J. Morgan and G .W. Watson, *J. Phys. Chem. C*, 2009, **113**, 7322.
21. C. J. Calzado, N. C. Hernández and J. F. Sanz, *Phys. Rev. B*, 2008, **77**, 045118.
22. M. Nolan, S. D. Elliott, J. S. Mulley, R. A. Bennett, M. Basham and P. Mulheran, *Phys. Rev. B*, 2008, **77**. 235424.
23. B. J. Morgan and G. W. Watson, *J. Phys. Chem. C,* 2010, **114***, 2321.*
24. N. A. Deskins, R. Rousseau and M. Dupuis, *J. Phys. Chem. C,* 2011, **115***,* 7562.
25. P. M. Kowalski, M. F. Camellone, N. N. Nair, B. Meyer and D. Marx, *Phys Rev Lett.*, 2010, **105**, 146405.
26. X. Gong and A. Selloni, *J. Phys. Chem. B*, 2005, **109**, 19560.
27. M. Liu, L. Piao, L. Zhao, S. Ju, Z. Yan, T. He, C. Zhou and W. Wang, *Chem. Commun.*, 2010, **46**, 1664.
28. W. Yang, J. Li, Y. Wang, F. Zhu, W. Shi, F. Wan and D. Xu, *Chem. Commun.*, 2011, **47**, 1809.
29. M. Lazzeri and A. Selloni, *Phys. Rev. Lett.,* **2001, 87***,* 266105.
30. H. Nakanishi, H. Morita and S. Nagakura, *Bull. Chem. Soc. Jpn.*, 1977, **50**, 2255.
31. K. Nakamoto, *Infrared and Raman Spectra of Inorganic and Coordination Compounds*, 4th ed.; Wiley-Interscience, New York, 1986.
32. Y. M. Wang, S. W. Liu, M. K. Lü, S. F. Wang, F. Gu, X. Z. Gai, X. P. Cui and J. Pan, *J. Mol. Catal. A: Chem.*, 2004, **215**, 137.
33. B. Schumacher, Y. Denkwitz, V. Plzak, M. Kinne and R. J. Behm, *J. Catal.*, 2004, **224**, 449.
34. H. Yang, Y. Hu, A. Tang, S. Jin and G. Qiu, *J. Alloys and Compounds* 2004, **363**, 271.
35. M. Ristic, M. Ivanda, S. Popovic and S. Music, *J. Non-Crystalline Solids*, 2002, **303**, 270.
36. P. V. Voort, M. G. White and E. F. Vansant, *Langmuir*, 1998, **14**, 106.
37. S. Haukka, E.-L. Lakomaa and T. Suntola, *Appl. Surf. Sci.*, 1994, **75**, 220.
38. H. Tada, H. Matsui, F. Shiota, M. Nomura, S. Ito, M. Yoshihara and K. Esumi, *Chem. Commun.*, 2002, 1678.
39. I. Sopyan, S. Murasawa, K. Hashimoto and A. Fujishima, *Chem. Lett.*, 1994, 723.
40. I. Sopyan, M. Watanabe, S. Murasawa, K. Hashimoto and A. Fujishima, *J. Photochem. Photobiol. A*, 1996, **98**, 79.
41. M. Nolan, *Chem. Comm.,* 2011, **46***,* 8617.
42. A. Iwaszuk and M. Nolan, *Phys. Chem. Chem. Phys.*, 2011, **13**, 4963.
43. C. M. Wang, A. Heller and H. Gerischer, *J. Am. Chem. Soc.*, 1992, **114**, 5230.
44. M. R. Hoffmann, S. T. Martin, W. Choi and D. W. Bahnemann, *Chem. Rev.*, 1995, **95**, 69.
45. H. Irie, K. Kamiya, T. Shibanuma, S. Miura, D. A. Tryk, T. Yokoyama and K. Hashimoto, *J. Phys. Chem. C*, 2009, **113**, 69.
46. V. E. Henrich and P. A. Cox, *The Surface Science of Metal Oxides*, Cambridge University Press, New York, 1994.
47. V. B. R. Boppana and R. F. Lobo, *ACS Catal.,* 2011, **1**, 923.